TECHNICAL MEMORANDUM

000

Model cycle upgrade from CY45R1 to CY46R1

ECMWF

November 22, 2018

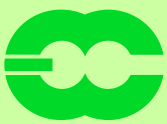

European Centre for Medium-Range Weather Forecasts
Europäisches Zentrum für mittelfristige Wettervorhersage
Centre européen pour les prévisions météorologiques à moyen terme

Series: ECMWF Technical Memoranda

A full list of ECMWF Publications can be found on our web site under:
http://www.ecmwf.int/en/research/publications

Contact: library@ecmwf.int

European Centre for Medium-Range Weather Forecasts
Shinfield Park, Reading, RG2 9AX, England

This document summarizes the key changes that are going to be introduced in cycle 46R1 and the main impact expected from this upgrade, which has been estimated on RD experimentation conducted so far. Cycle 46R1 is the result of the work of many RD people: their contributions are acknowledged.

1 Summary

Key changes

The key changes that are going to be introduced in model cycle 46R1 (compared to operations, model cycle 45R1) are:

- **Assimilation:**
  - Continuous data assimilation. Number of 4D-Var outer loops increased from 3 to 4. Early delivery assimilation window length increased from 6 to 8 hours. Observation cut off time extended.
  - Ensemble of Data Assimilations (EDA) increased from 25 members to 50 members.
  - Weakly coupled data assimilation introduced for sea-surface temperature in the tropics only.
  - Consistent spatial interpolation of the model to observation locations in trajectories and minimisations. Interpolation in nonlinear trajectories changed from bicubic to bilinear interpolation.
  - RRTOV upgraded from v12.1 to v12.2.
  - Updated Mie-tables generated using new permittivity model by Rosenkranz [2015].
  - Use of EDA to calculate Jacobians in soil moisture analysis.
- **Observations:**
  - Assimilation of SMOS neural network soil moisture product.
  - Assimilation of SSMIS-F17 150h GHz and GMI 166 v/h GHz.
  - Improved use of land sea mask in the field of view for microwave imagers.
  - Introduction of interchannel observation error correlations for ATMS.
  - Introduction of interchannel observation error correlations for geostationary water vapour channels.
  - Slant path calculations for geostationary radiances.
  - Extend usage of geostationary radiances to higher zenith angles.
  - Consistent infrared aerosol detection
- **Model:**
  - Improvements in convection scheme (entrainment, CAPE closure, shallow convection).
  - Activate LW scattering in radiation scheme.
  - 3D aerosol climatology replaces 2D climatology.
  - Correct scaling of dry mass flux in diffusion scheme.

  - Improvement of the TL/AD of the semi-Lagrangian departure point scheme in the polar cap area.
  - Fix instability in 2m temperature diagnostic related to wet tile.
  - Bug fix in the computation of rain amount that could freeze when intercepted by the snow-pack.
  - New physics for the wave model.
  - Limit on wave spectrum for very shallow water and minimum depth set to 3m.
  - Increase the frequency of the ensemble radiation timestep to 1 hour (from 3 hours).

- **Software/infrastructure:**
  -

Version	Merged Changes
v0	CY45R1, CY45R2, CY46
v1	Bit identical changes
v2	OOPS
v3	Neutral changes
v4	Data assimilation
v5	Physics and dynamics
v6	Coupled processes
v7	Continuous DA
v8	Late contributions

Table 1: List of the 46R1 incrementally merged versions

2 Testing and expected impacts for the medium-range forecasts

At the time of writing (1 November) the following 46R1 experiments have been run:

- winter and summer 4dVAR and forecasts (6 months in total all using the same EDA as input) at TCo399 resolution
- ENS forecasts:
  - TCo399, 20member testing initialised from research experiment and operational analysis
  - TCo399, 20member testing initialised from research experiment and operational analysis

Fig. 1 shows the difference of the own analysis root-mean-square errors (RMSE) in the 500 hPa geopotential height, for versions v3-v6 and 45R1 reference TCo399L137 forecasts, for summer 2017 and winter 2017-2018. These results indicate statistically significant error reductions for v6 in the extra-tropical region of both hemispheres of about 2% for almost the entire 10-day forecast range. The same plot is repeated for version v4, v5, v6 in Fig. 2, however, the forecasts are now verified against the operational analysis rather than own analysis. We notice that the combined effect of data assimilation and model changes give approximately same statistically significant reduction of the RMSE. Furthermore, a vertical cross-section of the RMSE difference against own analysis of v6-45R1 for the geopotential height field is given in Fig. 5.

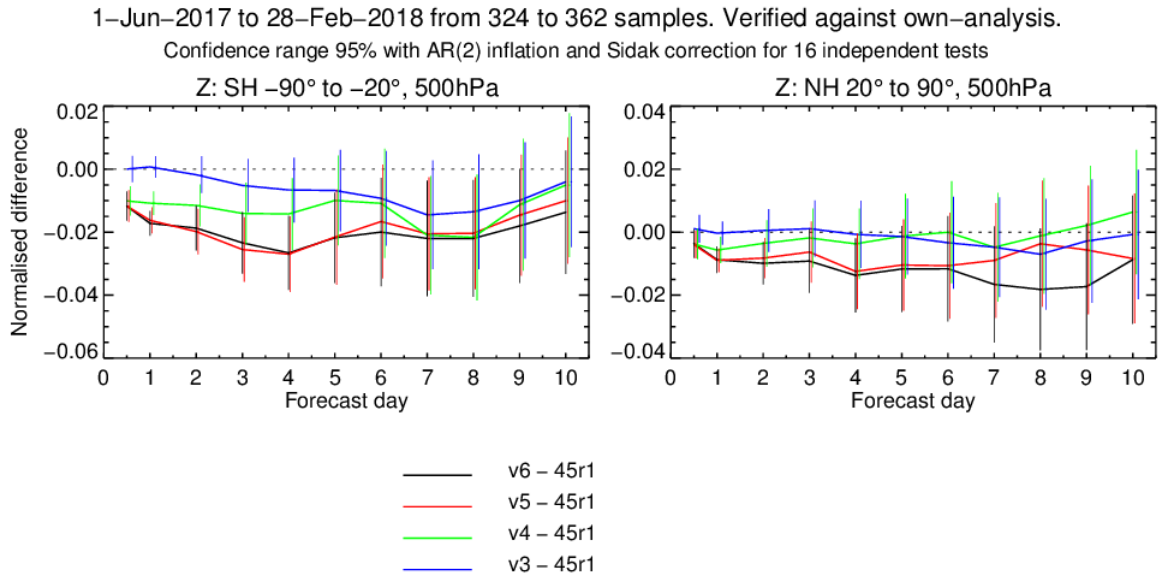

Figure 1: Normalized difference between the RMSE of the TCo399L137 forecasts run with 46R1 merged version v3-to-v6 and compared against 45R1. For the content of different versions see Table 1. Results are based on a combined summer/winter forecast run from 1 Dec 2017 to 28 Feb 2018 and 1 Jun 2017 to 31 Aug 2017.

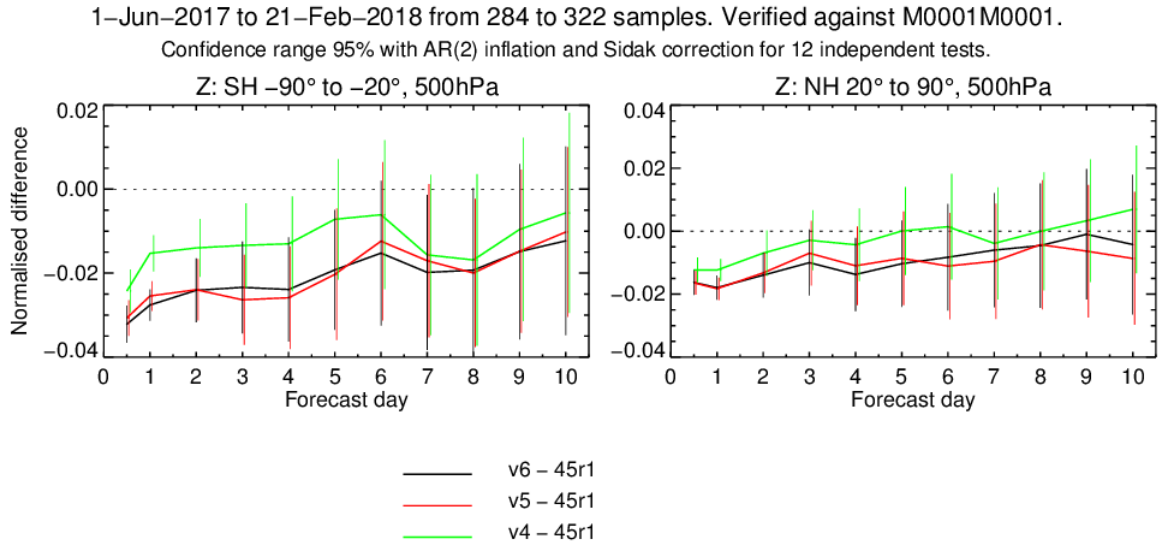

Figure 2: Same results as in Fig. 1 for v4, v5, v6 46R1 versions but verified against “independent” operational analysis.

Figure 3 shows fits to radiosonde temperature observations for the combined v3-v6 summer/winter Tco399L137 testing. There are no specific assimilation changes to radiosonde temperatures and so they represent a fairly independent measure of forecast accuracy. The large decrease in first guess relative standard deviations shows the combination of assimilation, observation usage, and physics changes are working in tandem to bring the model closer to the observations.

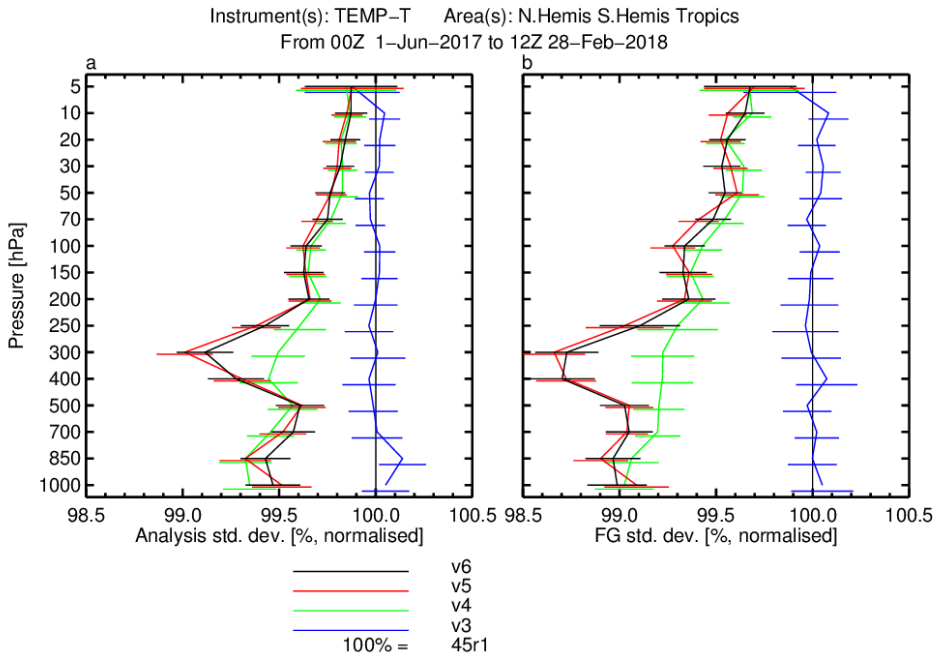

Figure 3: Analysis and first guess departures standard deviations for radiosonde temperature observations. We see improvements in first guess departures of the order of 0.3–1.3%. It is clear that the contributions from both assimilation (v4, green) and physics (v5, red) combine to better fit these observations relative to the previous CY45R1 baseline (100%).

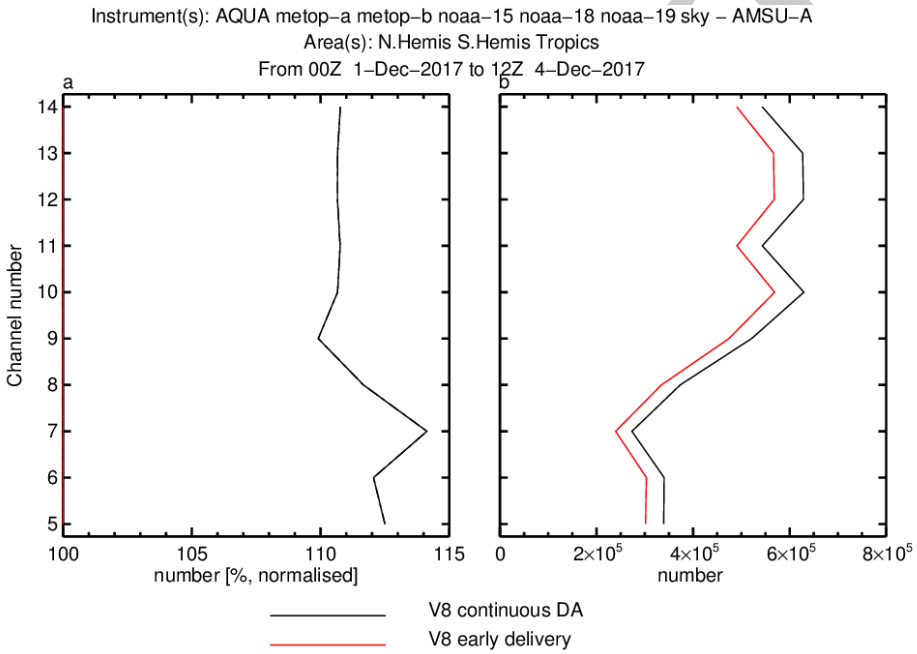

Figure 4: Observation increase for AMSU-A when going from the CY45R1 style early delivery system to the CY46R1 continuous DA early delivery system. The 10–13% increase in observation numbers is representative of the overall increase in observation numbers across all observation types. For each instrument however there is large variation in these numbers based on their dissemination procedures.

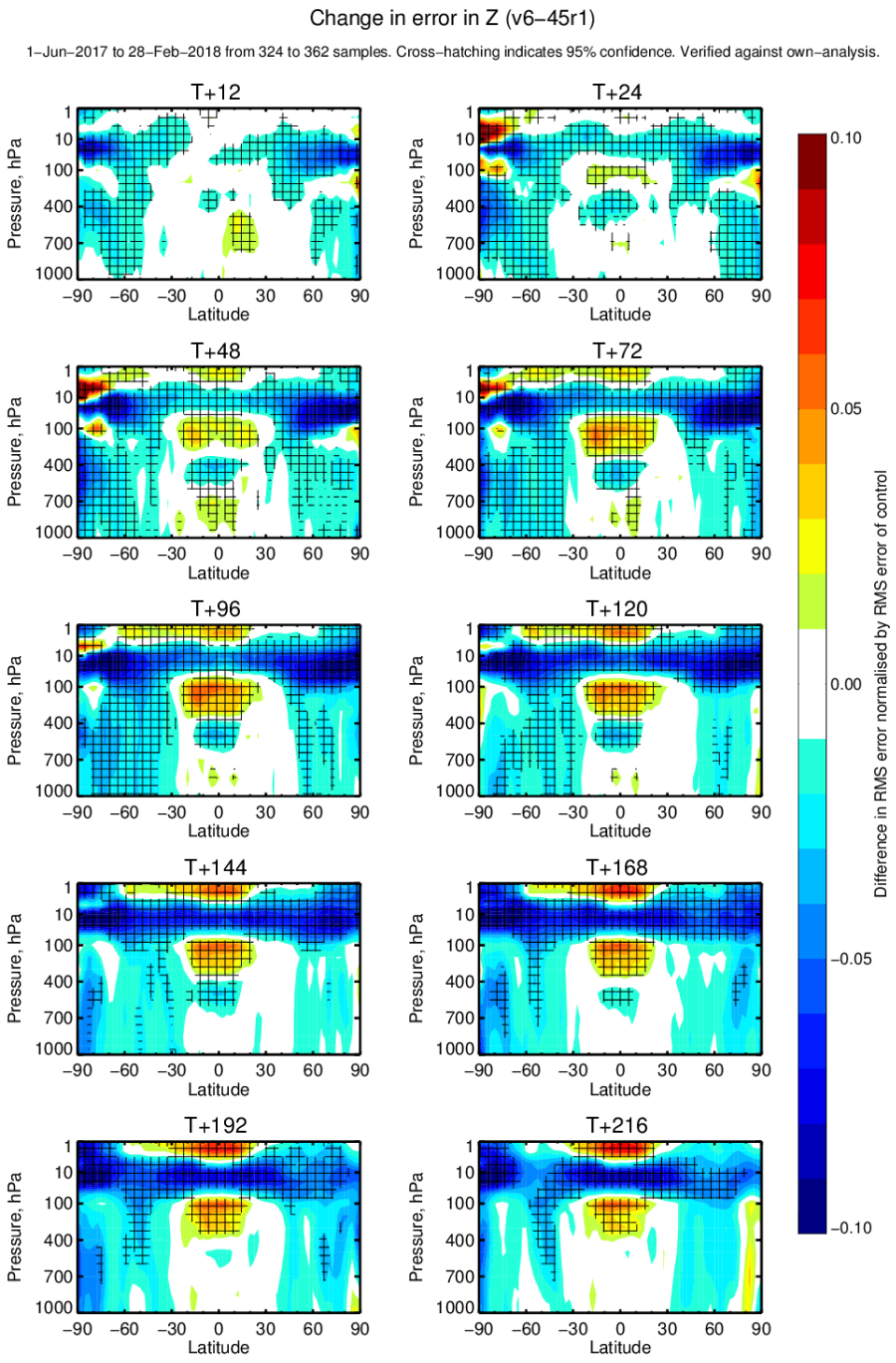

Figure 5: Combined summer/winter TCo399 difference in RMSE for Geopotential height as vertical cross-section comparing the merged model and data assimilation 46R1 contributions to the control 45R1 experiment. Blue colour indicating improvement and significance at 95% when gridded.

The impact on the ensemble scores of the combined model and ensemble changes (1 hour radiation) can be seen in Fig.6. We notice that the overall impact is positive. The apparent negative impact in the RMSE wave model fields (swh, mwp) is due to increased activity in the new scheme.

Figure 6: Combined summer/winter TCo399 ensemble scorecard for different meteorological fields. The 46R1 version including the merged model and data assimilation changes is compared with a baseline version which is equivalent (completely neutral) to 45R1. Green colours indicate improvement against the baseline version while red indicate deterioration.

3 Main contributions in data assimilation and observations

This cycle will include continuous data assimilation, a 50-member EDA, additional weak coupling of the atmospheric and ocean data assimilation systems. In data assimilation, a stronger coupling will be introduced between the atmosphere and the surface, with Jacobians computed from the EDA used in the surface analysis. Observation usage will be improved thanks to upgrades in the infrared and the microwave all-sky packages.

The Continuous Data Assimilation contributions allow use of later arriving observations, and crucially decouples the start time of the assimilation from the observational cut-off. This permits the beneficial introduction of an additional outer loop without affecting delivery time. Finally as part of the continuous data assimilation package, the early delivery assimilation window length has been increased from 6 hours to 8 hours, thus ensuring that *all* observations that have arrived can be assimilated.

The Ensemble of Data Assimilations (EDA) has increased from 25 to 50 members (with benefits to both the HRES and ENS) which was enabled by significant work on the efficiency of the system. In a progressive step in ocean–atmosphere weakly coupled assimilation, the atmospheric analysis sea-surface temperature in the tropics is now taken from the ECMWF OCEAN5-NRT analysis rather than using the OSTIA product directly.

The spatial interpolation of the model to observation locations in trajectories and minimisations has been made consistent. Interpolation in the nonlinear trajectories has been changed from bicubic to bilinear interpolation, resulting in better fits to observations as well as a slight improvement to computational efficiency.

The radiative transfer model RRTOV has been upgraded from v12.1 to v12.2. This is a broad scientific and technical upgrade to the microwave observation operators RTTOV and RTTOV-SCATT. The upgrade allows RTTOV to use the most accurate science possible, it prepares the way for future sensors like Ice Cloud Imager (ICI). Band corrections are implemented for all microwave sensors, improving accuracy of simulated microwave radiances. RTTOV-SCATT now does its radiative transfer in terms of radiance, not brightness temperature, improving accuracy by several tenths of a Kelvin in some channels (this also prepares the way for future mm-wave sensors like ICI). All-sky dynamic emissivity retrievals have been externalised and use a newly-provided RTTOV framework. This involves minor changes and improvements in the scientific basis of the retrieval, such as the use of the correct clear-sky emissivity in the clear-sky column. New Mie-tables are used that have been generated using the new permittivity model of Rosenkranz [2015]. There has been an update to the infrared aerosol detection channels, and re-specification of related tuning parameters to make them consistent for AIRS, IASI, and CrIS.

For the surface analysis of soil moisture, the Simplified Extended Kalman Filter (SEKF) has been significantly upgraded to improve the computational efficiency by computing its Jacobians directly from the EDA rather than with perturbed nonlinear trajectories. The SMOS neural network soil moisture product is now an additional observational input into the SEKF.

Cycle 46R1 has introduced a package of changes to microwave all-sky assimilation. This includes assimilation of SSMIS-F17 150h GHz and GMI 166 v/h GHz channels as well as improving the use of the land sea mask in the field of view for microwave imagers. Each Microwave observation has a footprint depending on its frequency. We use the 10GHz footprint for AMSR2 and GMI and the 19GHz footprint for SSMIS-FOV to compute how the land-sea mask is affected by this footprint. We name this land-sea mask “lsm_fov”, stored in odb space. lsm_fov is more accurate than the lsm used in CY45R1, which depends on the resolution of each loop. lsm_fov is then later used (if available) to decide if a superob is contaminated by land (not yet assimilated) or not (assimilated). 1% land contamination is allowed as it

has been identified to cause a change in brightness temperature of 1K, which is in the noise level of first guess departures.

Interchannel observation error correlations have been introduced for ATMS. The error covariance matrix is diagnosed using the Desroziers method from an experiment using a previously diagnosed matrix from the Hollingsworth-Lonnberg method (the same method was used to produce the IASI error covariance matrix implemented from cycle 43R1). The diagnosed error standard deviations are inflated by an empirically tuned factor of 1.75.

Similarly interchannel observation error correlations have been introduced for geostationary water vapour channels. The current instruments are: GOES IMAGER (1 WV channel), SEVIRI (Meteosat Second Generation) (2 WV channels), and AHI (Himawari) (3 WV channels). The Desroziers diagnostic R matrix has been computed for each of these instruments, and the resulting errors have been scaled by a factor of 6 in order to provide the best first guess fit to water vapour channels on other instruments (as well as impact at longer lead times). Further upgrades to the use of geostationary radiances is to extend their use to higher zenith angles (i.e. at the edge of the disk). At these high angles, line of sight of the satellite passes through a number of model columns. In order to improve the representation of these observations, the "slant path" method is used to perform the radiative transfer calculation along the line of sight. The configuration for CY45R1 used only vertical information from a single location. Currently, geostationary radiances are rejected in the blacklist if the satellite zenith angle is greater than 60 degrees. This change allows data to be used up to zenith angles of 74 degrees, thus improving coverage at the edges of the geostationary disks. This is particularly significant in the North Atlantic, where a significant amount of Meteosat-10 data is currently not being used.

This contribution updates the use of DBNet data with better timeliness (for AMSU-A and MHS). Addition of DBNet data from South American and New Zealand stations. Thinning to give preference to global rather than DBNet data for AMSU-A. Correction of azimuth angle provided in the data from some DBNet stations.

4 Main contributions in modelling

In 46R1 longwave scattering has been turned on, which leads to a slight warming of the surface and was found to lead to a modest reduction in the RMS error in tropospheric temperature forecasts by around 0.5%. A key innovation has been to represent longwave scattering by clouds but to neglect it for aerosols. This captures virtually all the benefits, and enables several optimizations to be performed achieving a neutral result in terms of computational cost. Furthermore, the 2D CAMS aerosol climatology has been replaced by a new 3D aerosol climatology. The latter better matches the original CAMS distribution and facilitates future updates of aerosol fields. The change has some positive impacts on lower tropospheric temperature and winds, especially along coastlines affected by seasonal biomass burning interacting with boundary layer clouds. Bigger positive impacts can be seen in the stratosphere where the RMSE of the temperature field in the 50-100 hPa layer near the summer pole decreases by 10% due to a similar reduction in the temperature bias.

The changes in the convection scheme include an increase in the entrainment of the test parcel, a positive definite correction for the denominator in the CAPE closure (improving the tangent-linear approximation) and for shallow convection a relative humidity dependent area fraction for evaporation (previously was a constant value).

A modification in the TL/AD of the semi-Lagrangian advection scheme results in improving the depar-

ture point calculation near the polar cap area. This was a long-standing problem, related with the way that inverse trigonometric functions were calculated in the non-linear and tangent-linear versions of the code. The latter was analytically but not discretely equivalent with the potential to give rise occasionally to an instability.

The changes introduced in the land surface scheme aim to minimize the occurrence of the maximum 2m temperature spikes - a side effect of an instability issue with the 2m temperature calculation. This was done by adjusting the wet tile skin conductivity. This modification partially solves the spike problem lowering the frequency of its occurrence by almost half. The increase in the skin conductivity for the interception tile (wet skin) is also justified from the physical point of view as a wet surface (basically thin water layer) should have higher conductivity than a dry one and the flux exchange should take the surface physical characteristics changes into account even for short living process. In addition a bit identical fix to the computation of the 2m temperature diagnostic for the wet skin and lakes tiles was introduced. All the performed experiments (forecast, 4D-Var and climate runs) suggested that the overall impact for such change is neutral to slightly positive.

Correctly accounting for the interception of rain has led to improved handling of episodically occurring snow events, since only a fraction of intercepted rain can refreeze. This has been introduced in 46R1 by correctly computing the amount of rain that could refreeze when intercepted by the snowpack. Previously, unphysical accumulation of snow in rainy conditions were locally observed during wintertime. Fig. 7 shows a case study in Bulgaria where only a small amount of snow was forecast at t+48 hours followed by a large amount of rain by t+96 hours. The experiment shows a reduction of snow water equivalent after t+96 while the control operational snow scheme showed increased snow with time. The change has been verified to have neutral impact on meteorological scores.

A new wave physics parameterisation for wind input and open ocean dissipation was implemented in CY46R1. It is based on the work of Ardhuin et al. [2010] and the initial implementation of it into the MeteoFrance version of the wave model code. It has been adapted and optimised to run efficiently with the latest version of the code. Because the wave model is coupled to the atmosphere, the new configuration was set up to yield similar level of feedback in the form of a sea state dependent Charnock coefficient. Note however, that the overall distribution of the Charnock parameter is bit tighter and yields slightly larger ocean surface roughness under typical tropical wind conditions. Impact on the ocean circulation, in the fully coupled system was also evaluated.

The main benefit of the changes is on the waves parameters, partly addressing the issue of over-prediction of long swell energy and the small under-estimation in the storm tracks. Fig. 8 shows the annual mean difference in significant wave height (SWH) between the new wave physics and the old. Generally, SWH is reduced in the deep tropics and enhanced in extra-tropics.

Output wave parameters available from ECMWF forecasting system comprise set of parameters for the description of the mean sea state, as well as descriptions of the different major wind sea and swell components (IFS documentation part VII, chapter 10). There is also a set of variables for the description of the single largest waves in a record, which when substantially larger than the mean state are commonly referred to as freak waves. Based on new shallow-water parametrizations of envelope skewness and kurtosis of the sea surface elevation due to waves Janssen [2017] and a new parametrization of dynamic kurtosis developed by Janssen and Janssen [2018], the freak wave parameter calculation has been updated. The main impact is an enhanced probability of larger waves in shallow water with respect to the old version.

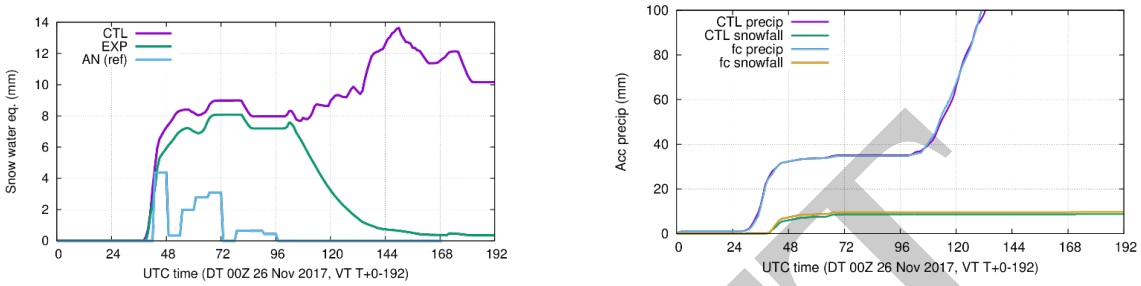

Figure 7: Left: time series of snow water equivalent for a site in Bulgaria (41.44N, 24.6E), for forecast experiments with the operational snow scheme (CTL), with the corrected (fix) snow scheme (EXP) and the operational analysis (AN) used as a reference. Forecasts are initialized 26 November 2017 at 00UTC. Right: same as in the left but for the accumulated total precipitation and snowfall. Note that the values for EXP are not displayed.

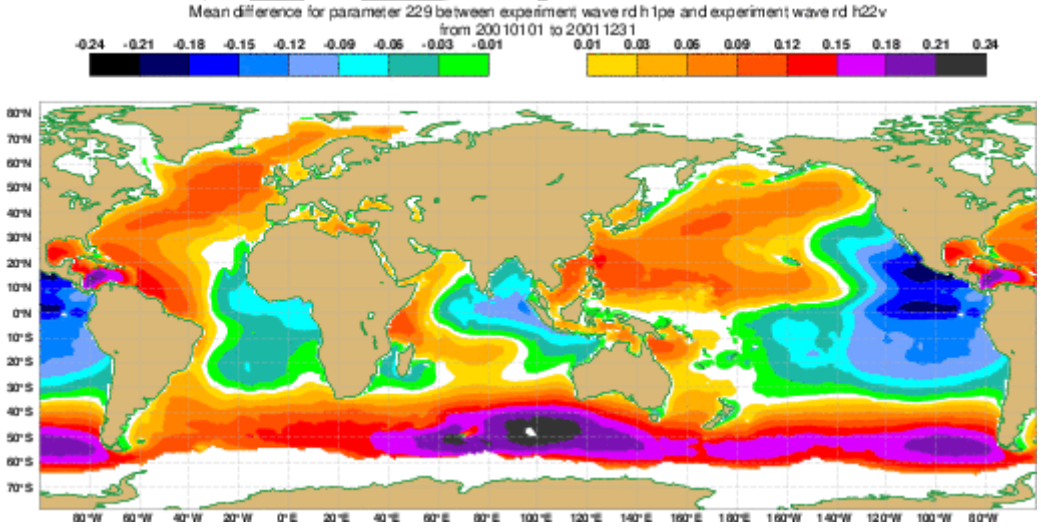

Figure 8: Annual mean difference in significant wave height (m) between the new and old wave physics. Data are from standalone wave model runs forced by ERA5.

5 Main contributions in ensemble configuration

In 46R1, the ensemble calls radiation every 1 hour as in HRES, rather than every 3 hours. The left plot in Fig. 9 shows that the forecast skill is improved almost everywhere, including an error reduction of up to 3% in 2m temperature. Note that this experiment tests the standard operational configuration of 50 members at full resolution TCo639 as opposed to the previous research experiments of section 2 where a "cheap" low resolution with reduced number of members set up is tested. Much of the improvement in the left plot of Fig. 9 can be attributed to the faster coupling of radiation, clouds and the surface, and indeed over tropical land areas the RMS error in low clouds has been reduced, by as much as 15% over Amazonia. More frequent radiation incurs an overall cost increase in the operational ENS of about 3%. This is possible in part because the new radiation scheme introduced in CY43R3 ECRAD is significantly cheaper than its predecessor.

A further change in the ensemble configuration is using 50-member EDA instead of a 25 member symmetric EDA and its impact can be seen in the right part of Fig. 9.

Figure 9: Left: Summer 50 member TCo639 ensemble scorecard for different meteorological fields comparing 1 hour radiation time step experiment against 3 hours radiation time step control experiment. Right: scorecard showing the impact of a 50 member ensemble experiment initialised by 50 member EDA against a control initialised by 25 member symmetric EDA. Green colours indicate improvement against the control while red indicate deterioration.

6 Extended range forecasts

Re-forecasts experiments with 46R1 v6 have been run once a month over the period 1989-2016 and 15 ensemble members. Although it is planned to use ERA5 to initialize the re-forecasts in 46R1, the experiments have been initialized from ERA Interim to isolate the impact due to the changes in model cycle.

Fig. 10 shows the MJO Index bivariate RMSE spread and error (left panel) and the amplitude error (right panel). The MJO Index forecast skill scores are not significantly different between cycles 46R1 and 45R1. However, the ensemble spread and the amplitude of the MJO are slightly lower in 46R1 than in 45R1. This degradation in ensemble spread and amplitude is statistically significant during the first 20 days of the re-forecasts.

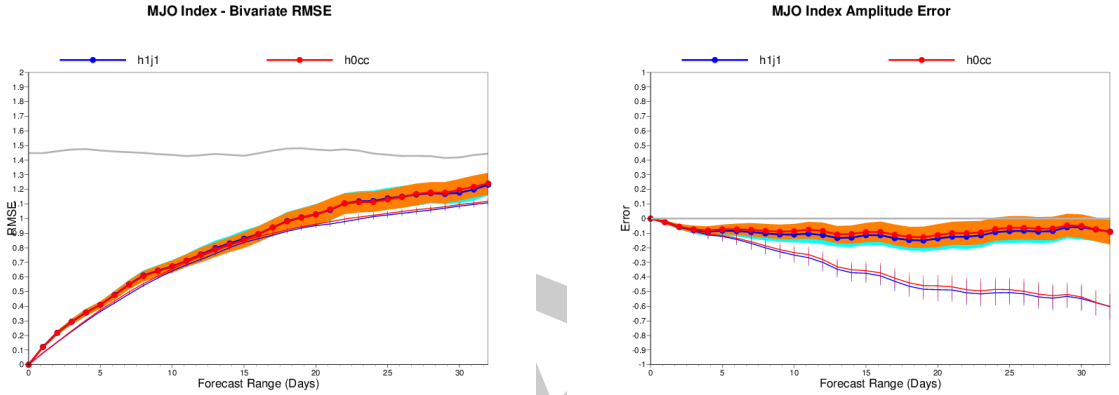

Figure 10: (a) MJO Index bivariate RMSE spread and error and (b) MJO Index amplitude error, as a function of forecast lead time in the ENS monthly system for Cycle 45R1 (red) and 46R1 version 6 (blue).

The RPSS skill scores (Fig. 11) for the monthly system are generally neutral across the range of parameters in the northern Extratropics. However, they indicate a small but statistically significant degradation for several parameters (mostly near-surface parameters) in the Tropics. This degradation could be linked to a slight, but statistically significant, reduction of the ensemble spread between cycle 46R1 and 45R1 for most of the variables in the Tropics as well as in the Extratropics (not shown).

7 Technical Changes

7.1 Limited set of ocean output in GRIB on the atmospheric grid.

New OCEAN GRIB parameters on the atmospheric grid in coupled mode:

- 174098 Ice thickness
- 151148 Mixed layer depth
- 151145 Sea level
- 151163 20 degree isotherm depth

- 151130 Sea surface salinity
- 151164 Mean temparature over 300m
- 151175 Mean salinity content over 300m

All fields are masked on land and lake points. 151164 and 151175 are masked on ocean points with depth $<$ 300m.

7.2 Operational implementation of EFI/SOT/CDFs for week-long periods of the extended-range forecast

This will include 2m temperature and total precipitation.

7.3 Optional dynamic extra field 212.250 to output dry deposition velocities

7.4 New archived fields from the EDA prost-processing for the land surface

With type `es` for steps 6 and 12 of each forecasts, with the following parameters:

139,140,236,39,170,171,42,40,183,184,237,41

7.5 New near-surface height levels for wind outputs

New hub-height wind outputs for wind energy applications. Currently we have only 100m wind - new levels to be added using same methodology. This will be for both ENS and HRES. Heights TBD.

7.6 New PV level at 1.5 units

Replicate the current products available on PV=2 level for PV=1.5, for both HRES and ENS

7.7 New climatology for probability of temperature anomalies

Climatology for the computation of probabilities of temperature anomaly greater than +4K, greater than +8K, less than -4K and less than -8K will be updated. At the moment, fixed outdated climatology is used. The new climatology will be based on re-forecasts (model climatology). This change will make these products up-to-date with what is used for other products such as the EFI, extended-range forecast anomalies and some new products such as probabilities of temperature anomalies above/below certain standard deviation thresholds.

The following 4 existing parameters will be modified:

- Temperature anomaly greater than +4 K (paramid: 131024)
- Temperature anomaly greater than +8 K (paramid: 131025)

- Temperature anomaly less than -4 K (paramid: 131023)
- Temperature anomaly less than -8 K (paramid: 131022)

7.8 Generating Process Identifier

- Atmospheric model: Updated from 149 to 150
- Ocean wave model Updated from 114 to 115
- HRES stand-alone ocean wave model Updated from 214 to 215

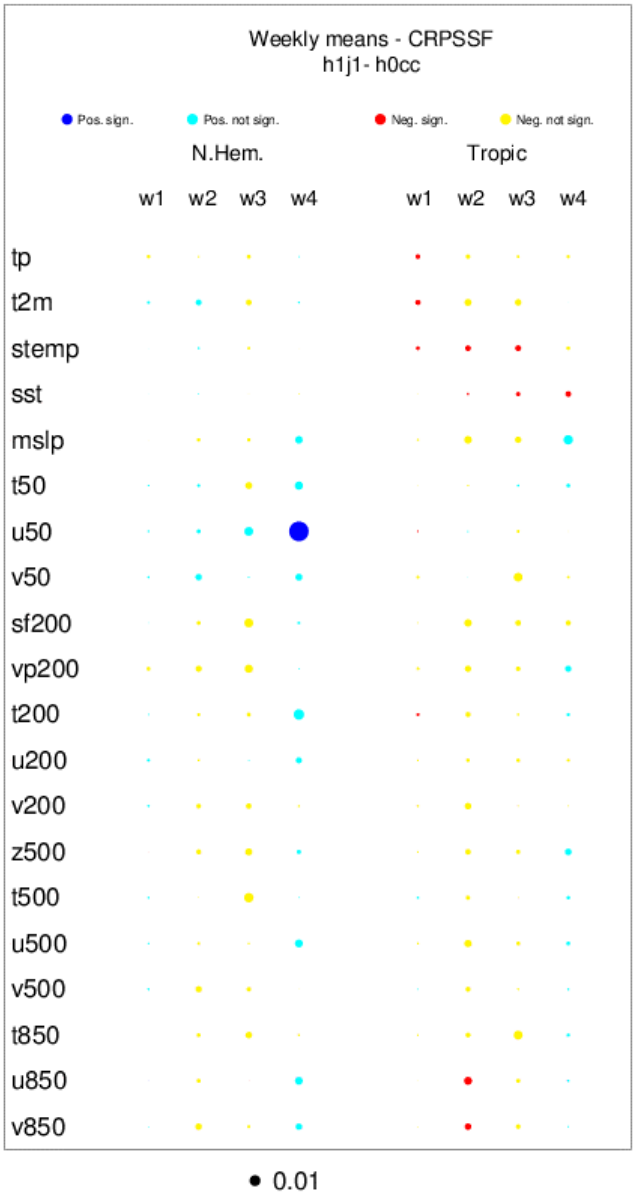

Figure 11: Annual mean difference in significant wave height (m) between the new and old wave physics. Data are from standalone wave model runs forced by ERA5.

A List of all 46R1 contributions

Fusce mauris. Vestibulum luctus nibh at lectus. Sed bibendum, nulla a faucibus semper, leo velit ultricies tellus, ac venenatis arcu wisi vel nisl. Vestibulum diam. Aliquam pellentesque, augue quis sagittis posuere, turpis lacus congue quam, in hendrerit risus eros eget felis. Maecenas eget erat in sapien mattis porttitor. Vestibulum porttitor. Nulla facilisi. Sed a turpis eu lacus commodo facilisis. Morbi fringilla, wisi in dignissim interdum, justo lectus sagittis dui, et vehicula libero dui cursus dui. Mauris tempor ligula sed lacus. Duis cursus enim ut augue. Cras ac magna. Cras nulla. Nulla egestas. Curabitur a leo. Quisque egestas wisi eget nunc. Nam feugiat lacus vel est. Curabitur consectetuer.

References

F. Ardhuin, E. Rogers, A. Babanin, J.-F. Filipot, R. Magne, A. Roland, A. van der Westhuysen, P. Queffeulou, J.-M. Lefevre, L. Aouf, and F. Collard. Semi-empirical dissipation source functions for wind-wave models: part i, definition, calibration and validation. *J. Phys. Oceanogr.*, 40(9):1917–1941, 2010.

P. Janssen. Shallow water version of the freak wave warning system. Technical Report 813, ECMWF, 2017.

P. Janssen and A. Janssen. Extreme ocean waves are a transient phenomenon. *J. Phys. Oceanogr.*, To appear, 2018.

P. W. Rosenkranz. A model for the complex dielectric constant of supercooled liquid water at microwave frequencies. *IEEE Trans. Geoscience and Remote Sensing*, 53(3):1387–1393, 2015.